Available online at www.sciencedirect.com
ScienceDirect
Scripta Materialia 60 (2009) 1109–1112
Scripta MATERIALIA
www.elsevier.com/locate/scriptamat

Effect of precipitate morphology evolution on the strength–toughness relationship in Al–Mg–Si alloys

S.P. Yuan,[a] G. Liu,[a] R.H. Wang,[a] G.-J. Zhang,[a] X. Pu,[a] J. Sun[a,*] and K.-H. Chen[b]

[a]*State Key Laboratory for Mechanical Behavior of Materials, School of Material Science and Engineering, Xi'an Jiaotong University, Xi'an 710049, China*
[b]*State Key Laboratory for Powder Metallurgy, The University of Southern Central China, Changsha 410083, China*

Received 24 January 2009; revised 13 February 2009; accepted 24 February 2009
Available online 27 February 2009

Experimental results show that the gradual evolution of precipitate morphology in Al–Mg–Si alloys, from spherical to rod-/needle-shaped, leads to an increase in ductility but a decrease in both yield strength and fracture toughness. The strength–ductility relationship reported here is similar to general observations but the strength–toughness relationship is distinctly different from the conventional one. These relationships are rationalized by considering a competition between dislocation–precipitate interaction and precipitate–matrix deformation discrepancy as the dominant strain localization mechanism, which is modulated by the evolution of precipitate morphology.

Keywords: Aluminum alloys; Fracture toughness; Precipitate; Morphology evolution

Both high strength and superior fracture toughness are required for heat-treatable aluminum alloys used in transportation fields such as in aircraft and automobiles [1–12]. The relationship between strength and fracture toughness has been a permanent focus of research into aged aluminum alloys. First, it is very useful for industrial purposes if toughness can be easily deduced from a tensile test using unnotched specimens and simple measurements. Second, a good understanding of this relationship can be favorable for artificially controlling the aging treatment to achieve a good combination of strength and fracture toughness. In general, the toughness of metals decreases as the strength is raised by alloying and heat treatment. The trade-off between strength and fracture toughness in heat-treated aluminum alloys is usually the result of aging treatment. From the under-aged conditions up until the peak-aged point, the increasing nucleation and growth of precipitates causes a successive enhancement in the strength. At the same time, the fracture toughness degrades gradually because the presence of fine precipitates induces local shear instability. In the over-aged conditions, where precipitates coarsen via Ostwald ripening, strength goes down and the fracture toughness can either go up or be almost unchanged, depending on the composition and fracture mode (intergranular or intergranular fracture) [5]. The known strength–fracture toughness relationships in aged aluminum alloys have mainly been explained based on the evolution of precipitate content and precipitate size with aging treatment [2–5]. However, the influence of precipitate morphology or precipitate shape on the strength–fracture toughness relationship is still unclear.

Most recently, the evolution of precipitate morphology, from spherical to predominantly rod- and needle-shaped, has been obtained in an Al–Mg–Si alloy by the present authors [13,14] using a two-step aging treatment. It has been found that the strength and ductility of the alloy were clearly affected by the evolution of precipitate morphology. In this paper, the influence of precipitate morphology evolution on the fracture toughness is investigated and the relationships between the mechanical properties, i.e. the strength–ductility and the strength–toughness relationships, are discussed in terms of this evolution.

The Al–Mg–Si alloy used in the present investigation is extruded rod 18 mm in diameter. The composition is 1.12 Mg, 0.57 Si, 0.25 Cu, 0.22 Cr (wt.%), and balance Al. The alloy had been solution-treated at 703 K for 30 min followed by water quenching and had then been

* Corresponding author. Tel.: +86 29 82667143; fax: +86 29 82663453; e-mail: junsun@mail.xjtu.edu.cn

1359-6462/$ - see front matter © 2009 Acta Materialia Inc. Published by Elsevier Ltd. All rights reserved.
doi:10.1016/j.scriptamat.2009.02.047

pre-aged at 373 K for 20 min. After storage at room temperature for 50 months, the alloys were secondarily aged at 473 K for a series of aging times (t) from 2 to 40 h. Yield strength (σ_y), reduction in area (RA%) and strain to fracture (ε_f) were measured in tension testing and details can be found in our previous paper [13,14]. Fracture toughness (KIC) was determined using three-point bending sample and J-integral measurement. The samples, 18 mm in width and 9 mm in thickness, have a L–R orientation (L, extrusion direction and R, radial direction) and the V-notch is normal to the extrusion direction. An initial crack was machined by spark erosion and subsequently grown by fatigue to an a/W value of 0.55–0.65 (a, crack length and W, sample width). Since the sample thickness is too small to obtain a valid KIC according to the ASTM standard, the ductile fracture toughness JIC was determined using the multiple-sample technique outlined by ASTM E813. An equivalent KIC, denoted KJC, was then derived from the JIC measurement using the relationship [15]:

$$K_{JC} = \left(\frac{J_{IC}E}{1-\nu^2}\right)^{1/2}, \quad (1)$$

where E (70 GPa) and ν (0.33) are the Young's modulus and Poisson's ratio of aluminum. For microstructural analyses, transmission electron microscopy (TEM) was used to determine the size and volume fraction of the precipitates. Details can be found in our previous papers [11,12,16,17].

Figure 1 shows the precipitate evolution with aging time (t) during the secondary aging treatment. At $t = 0$ or before the secondary aging treatment, the alloy contains spherical strengthening particles (Fig. 1b), which were determined to be the metastable pre-β″ phase of $AlMg_4Si_6$ [16], and were precipitated during the first aging treatment and subsequently grew during the subsequent storage period. In the secondary aging treatment, the spherical pre-β″ precipitates dissolved gradually. On the other hand, two other kinds of strengthening second-phase particles were precipitated, which are rod-shaped precipitates and needle-shaped precipitates, examples of which are shown in Figure 1c and d, respectively. The rod-shaped precipitates, which were determined to be the metastable β″ phase of Mg_5Si_6, formed in situ on the pre-β″ phase and grew by consuming the pre-β″ phase, while the needle-shaped strengthening particles, which were determined to be the metastable β′ phase of Mg_2Si, were precipitated from the matrix. The precipitation sequence is in good agreement with previous results [18]. During the entire secondary aging treatment, the volume fraction of spherical pre-β″ phase reduces progressively, while the volume fraction of rod-shaped β″ phase and needle-shaped β′ phase rises (Fig. 1a). However, there is not much change in the total volume fraction (about 1%) of the three kinds of precipitates. This means that, although the precipitate morphology changes gradually from fully spherical to predominantly rod- and needle-shaped, the evolution of precipitate morphology can simply be regarded as a conserved process because there is little change in the overall content.

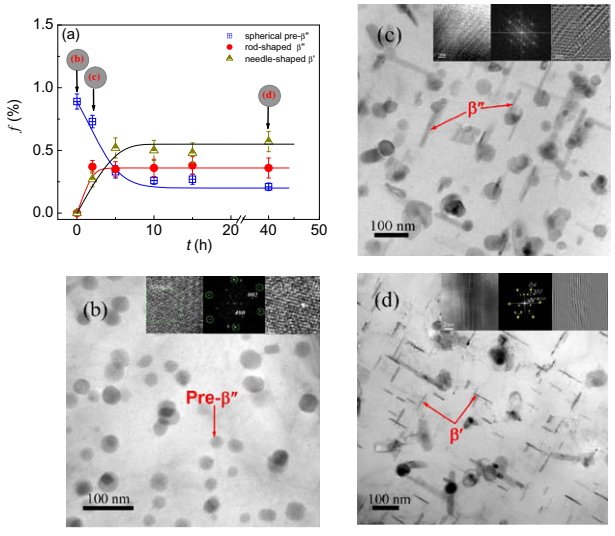

Figure 1. Evolution of precipitate volume fraction (a) and precipitate morphology (b–d) with aging time t. (b), (c) and (d) are typical TEM images of the alloy aged at $t = 0$, 2 and 40 h, respectively, to show the precipitate evolution from spherical pre-β″ precipitates of $AlMg_4Si_6$, to rod-shaped β″ precipitates of Mg_5Si_6 and needle-shaped β′ precipitates of Mg_2Si. Inserts in these images are structural analyses [14] for the three precipitates, respectively.

Table 1 summarizes the measurements of the mechanical properties. Variations in all these mechanical properties are obvious, along with the evolution of precipitate morphology. Prolonging the aging time or increasing t causes σ_y and K_{JC} to decrease while RA% and ε_f increase. The relationships between these mechanical properties will be discussed in detail by taking account of the evolution of precipitate morphology.

The strengthening effect in aged aluminum alloys mainly derives from precipitates. It is well known that raising the precipitate content and reducing the precipitate size can promote the strengthening effect. Furthermore, computer simulations have also revealed that precipitates with different shapes should have different strengthening responses [19]. According to our previous result [13,14], compared to rod-/needle-shaped precipitate, spherical precipitate has a stronger interaction with dislocation.

Strength and ductility are often mutually exclusive in a material. The pinning of dislocations, which induces strengthening, will cause local strain/stress concentration and degrade the deformation capability. A similar trend is found in the present aluminum alloys (Table 1), i.e. ductility increases while yield strength decreases, with the precipitate morphology changing from spherical to rod- and needle-shaped. Here, the parameters used to characterize ductility are ε_f and RA%, both derived from the measurement of area change. RA% is an important parameter, especially in industry, because it has significant implications in regard to bending and collapse. Lloyd [20] has proposed, based on a macroscopic model, that there exists a scaling relationship between RA% and σ_y in aluminum alloys. This scaling relationship was clearly found in 6000 series Al–Mg–Si alloys [20], where strength was varied by aging. Some data from 2000 series Al–Cu–Mg [11] and 6000 series Al–Mg–Si alloys [20] are shown in Figure 2a as square dots. RA% increases with reducing σ_y, and the relation-

Table 1. Measurements of the mechanical properties.

t (h)	σ_{ys} (MPa)	σ_{UTS} σ_{UTS} (MPa)	$RA\%$	n	ε_f	K_{JC} (MPa m$^{1/2}$)
0	255(±5)	330(±5)	8(±1)	0.142	0.08(±0.02)	36.79(±2.2)
5	228(±4)	308(±4)	19(±2)	0.141	0.17(±0.03)	36.15(±1.7)
10	215(±3)	293(±3)	21(±2)	0.123	0.19(±0.04)	32.75(±1.1)
30	205(±2)	272(±4)	23(±2)	0.117	0.21(±0.03)	32.43(±0.8)

ship is almost linear. The current results also show a scaling relationship – see the circular dots in Figure 2a. This indicates that the relationship between strength and ductility caused by the evolution of precipitate morphology is similar to previous observations.

However, the evolution of precipitate morphology does result in the strength–fracture toughness relationship being very different to traditional ones. Figure 2b gives the experimental results from some other researchers for conventional 2000 series Al–Cu–Mg alloys [3], 6000 series Al–Mg–Si alloys [21] and 7000 series Al–Zn–Mg alloys [2]. All three types of conventional heat-treated aluminum alloys exhibit fracture toughness (K_{IC} or UPE (the unit propagation energy in Kahn tear testing)) varying with yield strength in a reverse way. Conversely, the current results show that the fracture toughness varies directly with yield strength, as shown in Figure 2c. Because no visible changes were found in grain size, grain boundary and in the other two second-phase particles of constituents and dispersoids during the aging treatment, the unusual strength–fracture toughness relationship in the present experiments is ascribed to the evolution of precipitate morphology.

Precipitates generally have two effects on the fracture toughness of aged aluminum alloys [2]. On one hand, they increase the resistance to deformation, and thereby enhance toughness. On the other hand, the hardening caused by the precipitates is also accompanied by a tendency for slip localization, i.e. the development of superbands and large slip offsets which represent strain

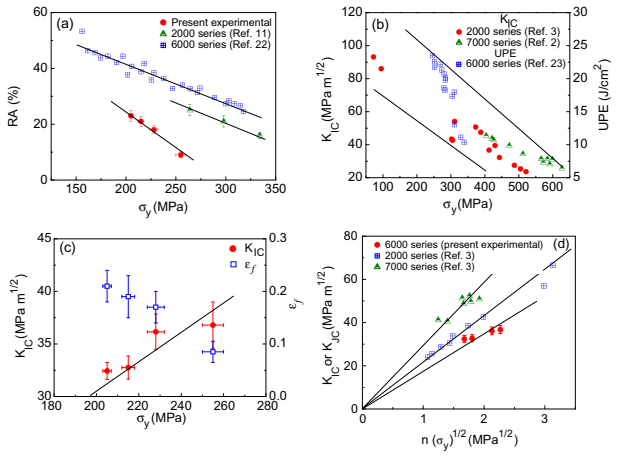

Figure 2. (a) Scaling of RA% with yield strength (σ_y) in the present alloy and previous 2000 series [11] and 6000 series [20] alloys. (b) Relationship between toughness (K_{IC} or UPE) and σ_y commonly observed in aged aluminum alloys, including 2000 series [3], 6000 series [21], and 7000 series [2]. (c) Dependence of K_{JC} and ε_f on σ_y in the present experiments.(d) Scaling of toughness with $n\sqrt{\sigma_y}$ in the present 6000 series, and previous 2000 series and 7000 series [3] aged aluminum alloys.

concentrations. Premature cracking within the strain concentrations leads to a loss of toughness. The yield strength of common heat-treated aluminum alloys is mainly varied by artificial aging, where the key is usually to control the precipitate content and precipitate size (for a mixed composition). Increasing the precipitate content (such as in the under-aged conditions) or reducing the precipitate size for the same content (such as by decreasing the aging temperature), can raise the yield strength. But, at the same time, these methods degrade both ductility and fracture toughness because they induce more intense slip localization.

In present experiments, however, the yield strength is changed by varying the precipitate morphology rather than by varying the precipitate content and size. The total volume fraction of the precipitates is almost unchangeable and the rod-shaped β″ precipitates are even nucleated directly on the spherical pre-β″ precipitates. In these conditions, the deformation capability and resistance to fracture of the alloys are mainly related to two effects: (i) the interaction between dislocations and precipitates; and (ii) the deformation compatibility between the elastic precipitates and the plastic matrix. As mentioned earlier, the dislocation interaction with spherical precipitates is stronger than that with rod-/needle-shaped precipitates, and so the spherical precipitates are more likely to cause local stress concentrations. On the other hand, applied stresses drive the aluminum matrix to deform plastically, while the hard precipitates embedded in the matrix cannot deform plastically but can be rotated [22]. Geometrically necessary dislocations have to be induced in order to make up for the deformation incompatibility between the precipitates and matrix [22]. Compared with the spherical precipitates, the rod-/needle-shaped precipitates have a much higher fraction of well-ordered surface, which makes ir more difficult to compensate for their deformation discrepancy.

A competition between the above two effects under different constraint conditions is responsible for the different trends observed here in strength–ductility and strength–fracture toughness relationships. In tensile testing of the smooth and unnotched samples, where the structural constraint is relatively low, the matrix can deform homogeneously throughout the sample (at least before the formation of necking). This continuous deformation allows the matrix to accommodate itself to the rotation of the rod-/needle-shaped precipitate and compensation for deformation incompatibility is not a problem. In this case, the deformation capability is controlled by the dislocation–precipitate interaction: the stronger this interaction, the larger the local strain concentration and thus the lower the deformation capability. Ductility decreases with increasing yield strength, as shown in Figure 2a. However, in testing the notched sample with large constraint, the plastic zone is localized

mainly ahead of the crack tip. In this case, the free deformation of the matrix is limited and it is difficult to compensate for the deformation discrepancy between the rod-/needle-shaped precipitates and matrix. Local stress/strain concentrations are thus induced in the precipitate–matrix interface, growing with further applied stress, and causing local strain concentration. In this case, the matrix–precipitate deformation discrepancy rather than the dislocation–precipitate interaction will be the dominant mechanism for local strain concentration. This enables the samples containing rod-/needle-shaped precipitates, although having lower strength, nevertheless to exhibit lower fracture toughness. From the above discussion, one can see that, with the precipitate morphology changing from spherical to rod- and needle-shaped, the reduction of fracture toughness is similar to that of yield strength, though their mechanisms are different.

Some previous studies of aluminum alloys have attempted to model the fracture toughness based on critical strain criteria for void formation [2,3,6] or critical stress criteria for matrix–particle decohesion [23]. Garrett and Knott [3] adopted the criterion that fracture will occur when the maximum strain ahead of the crack tip exceeds a critical value ε^* and suggested the following relationship for the effect of aging treatment on the fracture toughness of aluminum alloys:

$$K_{IC} \approx \sqrt{\frac{2CE\varepsilon^*\sigma_y n^2}{(1-\nu^2)}}, \tag{2}$$

where C is a constant (about 0.025) and n is the strain-hardening exponent. Chen and Knott [23] assumed that the fracture initiates when the tensile stress at the dispersoid–matrix interface exceeds the cohesive strength σ_c, which leads to the relationship that:

$$K_{IC} \approx \sqrt{\frac{mb}{10A} E\sigma_c\sigma_y n^2 \frac{\lambda}{d}}, \tag{3}$$

where m and A are constant, and λ and d are the average spacing and diameter of the dispersoids. After some modifications, such as replacing the parameters of dispersoid by those of precipitates, Eq. (3) can also be used to model the influence of precipitate–matrix interface decohesion on fracture toughness. Both Eqs. (2) and (3) reveal the correlation between K_{IC} and $n\sqrt{\sigma_y}$, i.e. $K_{IC}\alpha\ n\sqrt{\sigma_y}$, which has been directly verified by experimental results, such as shown in Figure 2d for 2000 and 7000 series alloys [3]. Since the variation in n with aging runs counter to the dependence of yield strength on heat treatment, the combination of n and σ_y as described in Eqs. (2) and (3) was considered to provide a better understanding of correlation between fracture toughness and tensile properties (Fig. 2b vs. 2d). The current results, although exhibiting a strength–fracture toughness relationship different from the conventional one, follow a similar scaling law between K_{IC} and $n\sqrt{\sigma_y}$, as commonly observed and analytically predicted. This indicates that the relationships between mechanical properties are essentially identical to some degree, no matter whether the relationships are varied by changing the precipitate content, size or morphology.

In summary, the influences of precipitate morphology evolution on the mechanical properties were studied in aged Al–Mg–Si alloys. When the precipitate shape changed from fully spherical to predominantly rod-/needle-shaped, the ductility of alloys increases but yield strength and fracture toughness both reduce. The current strength–ductility relationship (ductility varying inversely with strength) is similar to previous observations but the strength–toughness relationship (toughness increasing with increasing strength) is opposite to the conventional one. These relationships can be explained by considering a competition between dislocation–precipitate interaction and matrix–precipitate deformation discrepancy as the main strain localization mechanism, which is modulated both by the evolution of precipitate morphology and by the constraint conditions.

This work was supported by the National Basic Research Program of China (Grant No. 2004CB619303 & 2005CB623700), the National Natural Science Foundation (50701035) and the National Outstanding Young Investigator Grant of China. This work was also supported by the 111 Project of China under Grant No. B06025,

[1] E. Hornbogen, E.A. Starke Jr., Acta Metall. 41 (1993) 1.
[2] G.T. Hahn, A.R. Rosenfield, Metall. Trans. 6A (1975) 653.
[3] G.G. Garrett, J.F. Knott, Metall. Trans. 9A (1978) 187.
[4] D.S. Thompson, Metall. Trans. 6A (1975) 671.
[5] S. Suresh, A.K. Vasudevan, M. Tosten, P.R. Howell, Acta Metall. 35 (1987) 25.
[6] R.H. Van Stone, J.A. Psioda, Metall. Trans. 6A (1975) 668.
[7] J.T. Staley, Aluminum 55 (1979) 277.
[8] S. Esmaeili, D.J. Lloyd, W.J. Poole, Acta Mater. 51 (2003) 3467.
[9] M.J. Starink, S.C. Wang, Acta Mater. 51 (2003) 5131.
[10] D. Dumont, A. Deschamps, Y. Brechet, Mater. Sci. Eng. A356 (2003) 326.
[11] G. Liu, J. Sun, C.W. Nan, K.H. Chen, Acta Metall. 53 (2005) 3459.
[12] G. Liu, G.J. Zhang, R.H. Wang, W. Hu, J. Sun, K.H. Chen, Acta Metall. 55 (2007) 273.
[13] S.P. Yuan, G. Liu, R.H. Wang, X. Pu, G.J. Zhang, J. Sun, K.H. Chen, Scripta Mater. 57 (2007) 865.
[14] S.P. Yuan, G. Liu, R.H. Wang, G.J. Zhang, X. Pu, J. Sun, K.H. Chen, Mater. Sci. Eng. A499 (2009) 387.
[15] J.A. Begley, J.D. Landes, in: Fracture Toughness, Proceedings of the 1971 National Symposium on Fracture Mechanics, Part II, ASTM STP 514, American Society for Testing and Materials, Philadelphia, PA, 1972, pp. 1–20.
[16] G. Liu, G.J. Zhang, X.D. Ding, J. Sun, K.H. Chen, Mater. Sci. Eng. A344 (2003) 113.
[17] G. Liu, G.J. Zhang, X.D. Ding, J. Sun, K.H. Chen, Metall. Mater. Trans. 35A (2004) 1725.
[18] H.W. Zandbergen, S.J. Andersen, J. Jansen, Science 277 (1997) 1221.
[19] A.W. Zhu, E.A. Starke Jr., Acta Mater. 47 (1999) 3263.
[20] D.J. Lloyd, Scripta Mater. 48 (2003) 341.
[21] R.C. Dorward, C. Bouvier, Mater. Sci. Eng. A254 (1998) 33.
[22] M.F. Ashby, Philos. Mag. 21 (1970) 399.
[23] C.Q. Chen, J.F. Knott, Mater. Sci. 15 (1981) 357.